

# Accelerated MR Cholangiopancreatography with Deep Learning-based Reconstruction

Jinho Kim<sup>1,2</sup>, Marcel Dominik Nickel<sup>2</sup>, and Florian Knoll<sup>1,3</sup>

<sup>1</sup>Artificial Intelligence in Biomedical Engineering, Friedrich-Alexander-Universität Erlangen-Nürnberg, Germany, <sup>2</sup>MR Application Predevelopment, Siemens Healthineers AG, Forchheim, Germany, <sup>3</sup>Center for Advanced Imaging Innovation and Research (CAI<sup>2</sup>R), Department of Radiology, New York University Grossman School of Medicine, New York, NY, USA

## Abstract

### Purpose

To accelerate MR cholangiopancreatography (MRCP) acquisitions using deep learning-based (DL) reconstruction at 3T and 0.55T.

### Methods

Thirty healthy volunteers underwent conventional two-fold MRCP scans at field strengths of 3T or 0.55T. We trained a variational network (VN) using retrospectively six-fold undersampled data obtained at 3T. We then evaluated our method against standard techniques such as parallel imaging (PI) and compressed sensing (CS), focusing on peak signal-to-noise ratio (PSNR) and structural similarity (SSIM) as metrics. Furthermore, considering acquiring fully-sampled MRCP is impractical, we added a self-supervised DL reconstruction (SSDU) to the evaluating group. We also tested our method in a prospective accelerated scenario to reflect real-world clinical applications and evaluated for its adaptability to MRCP at 0.55T.

### Results

Our method demonstrated a remarkable reduction of average acquisition time from 599/542 to 255/180 seconds for MRCP at 3T/0.55T. In both retrospective and prospective undersampling scenarios, the PSNR and SSIM of VN were higher than those of PI, CS, and SSDU. At the same time, VN preserved image quality of undersampled data, i.e., sharpness and the visibility of hepatobiliary ducts. In addition, VN also produced high quality reconstructions at 0.55T resulting in the highest PSNR and SSIM.

### Conclusion

VN trained for highly accelerated MRCP allows to reduce the acquisition time by a factor of 2.4/3.0 at 3T/0.55T while maintaining the image quality of the conventional acquisition.

## Introduction

Magnetic resonance cholangiopancreatography (MRCP) is a non-invasive imaging modality for the diagnosis of diseases of the hepatobiliary system, providing a detailed view of the ductal system and pathologies [ [1], [2], [3], [4]]. Initially performed using 2-D thick-slice techniques, MRCP has evolved to 3-D imaging to improve image quality and provide comprehensive multidimensional views. However, these improvements have resulted in longer acquisition times, leading to motion artifacts [5]. There are two methods to address these challenges: Breath-hold and triggered free-breathing acquisitions. However, due to the constraint of breath-holding, the triggered free-breathing acquisition method is more practical in clinical applications.

Triggered techniques allow patients to breathe naturally throughout the scan while effectively minimizing motion artifacts caused by breathing. The prospective acquisition correction (PACE) technique has significantly enhanced the quality of triggered free-breathing 3-D MRCP. Compared to conventional respiratory-based triggering methods, the PACE triggering method produces fewer motion artifacts and images with sharper anatomical contours [6]. Furthermore, Asbach et al. [7] highlighted that PACE-triggered free-breathing 3-D MRCP (PACE-MRCP) significantly improves the visualization of hepatobiliary and pancreatic ductal structures compared to breath-holding 3-D MRCP, providing more detailed images. In addition, PACE-MRCP serves patient comfort during the scan. Despite these advantages, PACE-MRCP sometimes requires long acquisition times due to irregular breathing patterns.

To address the challenge of long acquisition times in PACE-MRCP, recent studies have focused on accelerating the k-space data acquisition [8]. This acceleration is typically achieved by undersampling the k-space data, which is effective in reducing acquisition time but introduces the risk of aliasing artifacts. To address these artifacts, various reconstruction methods, such as parallel imaging (PI) and compressed sensing (CS), have been developed [ [9], [10]]. PI significantly reduces the scan time by exploiting the correlations between multiple coil sensitivity profiles [11]. CS leverages the incoherence in undersampling patterns, which leads to uncorrelated aliasing artifacts, and enables image reconstruction from highly undersampled and sparse k-space data [12].

Furthermore, deep learning-based (DL) reconstruction methods have gained popularity in MR reconstruction [13], especially physical model-driven DL reconstruction methods. These physical model-driven DL reconstruction methods solve the traditional iterative optimization problems in an unrolled manner through multiple iterations. These DL reconstruction approaches determine model parameters based on multiple training data and reconstruct unseen data in an inference step. These DL reconstruction models can be viewed as generalized functions mapping undersampled data to high quality reconstructions. These methods have shown remarkable performance in the reconstruction tasks of highly accelerated MRI [ [14], [15]].

A variational network (VN) [14] is a supervised training method requiring fully sampled ground truth. However, acquiring fully sampled data, especially for MRCP, is challenging. To overcome this problem, a self-supervised training method, SSDU (self-supervised learning via data undersampling) [15] has been proposed. However, given the common use of accelerated MRCP in clinical settings, it is possible to train VN using conventionally accelerated MRCP as a substitute for fully sampled data. Therefore, it is worth to compare between supervised training and self-supervised training in the context of accelerated MRCP.

The generalization of DL reconstruction models is a field of high relevance as it determines the range of validity and the requirements on the training data. First works investigated the domain shift between field strengths that cause different signal-to-noise ratio (SNR) levels in reconstructions [16]. In addition, when the noise level affects the reconstructions much more than aliasing artifacts, the DL reconstruction model focuses more on denoising than aliasing artifacts removal [14]. In this regard, considering the importance of low-field MRI that has entered the clinical stage in recent years, although it produces a low SNR in reconstructions [17], DL reconstruction model can suppress the noise level of low-field MRI while reducing acquisition time.

This study aims to reduce MR acquisition time for PACE-MRCP while preserving image quality, especially intricate details of the hepatobiliary and pancreatic ductal systems. We perform this study using retrospective data and extend the retrospective study to the prospective setting to reflect real-world clinical applications. Furthermore, we evaluate the generalization of the obtained VN between different field strengths on PACE-MRCP for both retrospective and prospective undersampling.

## Theory

### MRI Reconstruction

The MRI reconstruction model can be expressed as

$$y = \mathbf{E}x + n, \tag{1}$$

where  $x$  is the final image to be recovered,  $y$  the acquired  $k$ -space data, and  $n$  the noise. The linear encoding operator  $\mathbf{E}$  includes the coil sensitivity map matrix, the Fourier transform operator and an undersampling matrix. In general, the reconstruction of accelerated MRI is an ill-posed problem, and the solution can be obtained by incorporating regularizers that provide prior information to the objective reconstruction function. Then, the regularized optimization problem can be formulated as

$$\operatorname{argmin}_x \|y - \mathbf{E}x\|_2^2 + \lambda \mathcal{R}(x), \tag{2}$$

where  $\mathcal{R}$  is a regularization operator, and  $\lambda > 0$  is a regularization parameter to balance the data fidelity and the regularization terms. Classical choices of  $\mathcal{R}$  include the  $\ell_1$ -norm of wavelet coefficients [ [12], [18]] and the  $\ell_2$ -norm of intermediate reconstructions [19].

In DL reconstruction, Equation ( 2 ) is solved by unrolling it with a fixed number of iterations [20]. Then the neural network plays a role as derivative of the regularizer  $\mathcal{R}$  in the gradient descent updating scheme for Equation ( 2 ) as

$$x^{i+1} = x^i - \alpha \left( \mathbf{E}^*(\mathbf{E}x^i - y) + \mathcal{N}_\theta^i(x^i) \right), \tag{3}$$

where  $x^0$  is the initial reconstruction of the SENSE-based  $k$ -space data,  $\alpha$  a step size,  $\mathbf{E}^*$  the adjoint linear operator, and  $\mathcal{N}_\theta^i$  the output of the neural network parameterized with  $\theta$  at iteration  $i \in [0, \dots, N - 1]$  and the fixed number of iterations defined as  $N$ .

## Training Manners of Deep Learning-based MRI Reconstruction

### Supervised Learning

In a supervised training manner, the DL reconstruction model is trained with training data  $\{(x_{ref}^i, y^i) : i = 0, \dots, M - 1\}$ , where  $M$  denotes the number of training data,  $x_{ref}^i$  and  $y^i$  are the ground truth image and the undersampled k-space data at the  $i$ -th pair, respectively. In general,  $x_{ref}^i$  is a fully-sampled reconstruction. DL reconstruction for supervised learning can be expressed as

$$\operatorname{argmin}_{\theta} \frac{1}{M} \sum_{i=0}^{M-1} \mathcal{L}(x_{ref}^i, f(y^i, \mathbf{E}^i; \theta)), \quad (4)$$

where  $f(y^i, \mathbf{E}^i; \theta)$  denotes the output of the unrolled network that is parameterized by  $\theta$ , and  $\mathcal{L}(\dots)$  the loss function between the ground truth and the network output. Thus, the network learns the model parameters  $\theta$  using the fully-sampled reference to minimize the average loss over the full set of training data. In the case of VN, the loss function is defined as structural similarity loss.

### Self-supervised Learning

Since the acquisition of fully-sampled reconstructions is not trivial or impossible in many medical conditions, mainly due to the long scan time, training the model in a self-supervised manner can be an alternative. The SSDU (self-supervised learning via data undersampling) [15] splits the undersampled k-space data into two subsets for training and loss calculation as

$$\Omega = \Theta \cup \Lambda, \quad (5)$$

where the undersampled data indices  $\Omega$  include both data index subsets of  $\Theta$  and  $\Lambda$ , being disjoint from  $\Theta$  and  $\Lambda$ . Then, the MRI reconstruction can be expressed as

$$\operatorname{argmin}_{\theta} \frac{1}{N} \sum_{i=1}^N \mathcal{L}(y_{\Lambda}^i, \mathbf{E}_{\Lambda}^i (f(y_{\Theta}^i, \mathbf{E}_{\Theta}^i; \theta))), \quad (6)$$

where  $f(y_{\Theta}^i, \mathbf{E}_{\Theta}^i; \theta)$  is the unrolled network output image using k-space data only at  $\Theta$  indices. Then, the output image is transformed into  $k$ -space data using the encoding operator  $\mathbf{E}_{\Theta}^i$ , specified by the  $\Lambda$  indices. SSDU defines the loss function as the combination of  $\ell_1$ - $\ell_2$  norm that is calculated between the subset  $y_{\Lambda}^i$  and the output k-space at  $\Lambda$  locations.

## Materials and Methods

### MRCP Data Acquisition

From February 2023 to February 2024, we collected MRCP data from 30 healthy volunteers (19 males and 11 females). All participants received an informed consent discussion and gave their written informed consent for their data being further used and processed. Mean age of the participants was 57.6, ranging from 20 to 81. Twenty-six out of the 30 volunteers were scanned at a field strength of 3T

(MAGNETOM Vida and Lumina, Siemens Healthineers AG, Forchheim, Germany), and four volunteers at a field strength of 0.55T (MAGNETOM Free.Max, Siemens Healthineers AG, Forchheim, Germany). We employed multi-channel coil arrays for imaging, consisting of an 18-/12-/9-channel body array and a 36-/24-/6-channel spine array, for the Vida (3T), Lumina (3T), and Free.Max (0.55T) scanners. The volunteers were positioned in the supine, head-first orientation during the scan. We acquired 3-D MRCP data using a 3-D T2-weighted turbo spin-echo sequence (SPACE) [21] in a free-breathing acquisition technique with the PACE triggering method for motion management. We averaged MR signals for 1.4 and 2 times for 3T and 0.55T scanner systems, respectively, to compensate the free induction decay (FID) artifacts, and this averaging process is common for the SPACE sequence [22]. Furthermore, we accelerated MRCP acquisition by factors of  $R=2$  and  $R=6$  along the phase encoding direction. Notably, we conducted multiple scans of volunteers, included in the training dataset, by varying the field-of-view. Table 1 shows detailed scan parameters.

### Raw Data Processing

We completed the conversion of the raw data to the ISMRMRD format [23] using the ISMRMRD<sup>1</sup> Python toolbox. We converted 3-D  $k$ -space data to a 2-D format by applying an Inverse Fourier Transform (IFT) along the fully-sampled slice (partition) direction. We performed a volume-wise normalization on the stack of 2-D  $k$ -space data to ensure consistent data scaling across volumes. Then, we undersampled the initial two-fold accelerated MRCP data by an additional factor of three to generate the six-fold undersampled input to train the network.

Furthermore, we conducted the estimation of the coil sensitivity maps using the ESPIRiT algorithm [24] as part of our preliminary steps using the Sigpy Python package [25] with a  $24 \times 24$  fully-sampled center  $k$ -space block and a  $5 \times 5$  kernel. Contrary to the default parameter in Sigpy, we did not crop the background out to zero in the image domain. We maintained consistency for all reconstructions in this study using the same predefined coil sensitivity maps.

### Deep Learning-based Reconstruction

#### Dataset Split

We divided our group of 30 volunteers into three independent sets for our study. The training and validation datasets included 17 volunteers and one volunteer, all scanned at 3T and were six-fold retrospective undersampling. Due to multiple scans of volunteers in the training dataset, the training dataset included 38 data volumes. The test dataset included the remaining 12 volunteers, eight scanned at 3T and four scanned at 0.55T. For the test dataset, we applied two distinct undersampling approaches, both at a reduction factor of  $R=6$ : retrospective undersampling and prospective undersampling. We used a GRAPPA reconstruction [26] of the  $R=2$  data to obtain a ground truth for the training of the supervised DL networks.

#### Network Architectures

We built our supervised model architecture upon VN [14] using a U-Net with four encoding and decoding layers [27]. Instead of using zero-filled  $k$ -space data as the input to the network, we performed an initial SENSE reconstruction and used that as the input to our network architecture. We employed pre-estimated coil sensitivity maps [24] for both SENSE initialization and VN processing. Figure 1 shows the entire VN training pipeline. In parallel to the supervised model, we also trained a self-supervised

---

<sup>1</sup> <https://pypi.org/project/ismrmrd/>

model, SSDU [15] based on Res-Net with 15 residual blocks [28]. Since we focused on the training schemes of supervised and self-supervised learning rather than the network models, we kept the initially proposed network models for both VN and SSDU. We used the same retrospective undersampling of R=6 as for VN to train SSDU. We trained VN and SSDU using the same Adam optimizer with 12 unrolling steps but different learning rates of 0.001 for VN and 0.0005 for SSDU and loss function of SSIM loss for VN and  $\ell_1$ - $\ell_2$  loss for SSDU.

### Conventional Reconstruction

We implemented iterative parallel imaging (CG-SENSE) [19] and compressed sensing (CS) [12] using the Sigpy Python package [25]. To find the optimal regularization parameters for both CG-SENSE and CS reconstructions, we initially set these parameters to values that maximized the SSIM with respect to the ground truth. Subsequent adjustments were made to enhance image perception quality, resulting in final parameter values of 0.01 for CG-SENSE and 0.1 for CS, respectively.

### Evaluation

We assessed our method through quantitative and qualitative comparisons, comparing with CG-SENSE, CS, and SSDU. In the retrospective study, we computed peak signal-to-noise ratio (PSNR) and structural similarity (SSIM) metrics in the test dataset. These metrics were computed on the magnitude-valued 3-D reconstruction volume, specifically the stack of the absolute-valued 2-D reconstructions, after min-max normalization to the 3-D volume. VN and the other reconstructions, such as CG-SENSE, CS, and SSDU, on retrospective undersampling at R=6 were compared to the GRAPPA reconstruction at R=2. We also calculated the average PSNR and SSIM over 12 test datasets, eight for 3T and four for 0.55T. We then performed a paired t-Test to prove statistical significance of our proposed method against reconstructions in the comparison group in terms of PSNR and SSIM. A  $p$ -value of less than 0.05 was considered statistically significant. In the prospective study, due to the lack of the ground truth, we compared reconstructions in terms of image quality.

In addition, we obtained line profiles from reconstructions to analyze details of the hepatobiliary ducts as well as the presence of residual aliasing artifacts. The line profile was derived from the end of the common bile duct, which we manually selected based on the maximum intensity projection (MIP) image of the 3-D reconstructed volume. Moreover, we calculated the Pearson product-moment correlation coefficient (PPMCC) [29] of the line profiles for all reconstructions with respect to the GRAPPA reconstruction at R=2. The PPMCC serves as a measure of similarity, with values closer to one indicating a higher degree of similarity between two profiles.

### Hardware and Tools

All experiments were conducted on a system equipped with an AMD Rome 7662 CPU 2.0 GHz, 512 GB of RAM, and an NVIDIA Tesla A100 SXM4 with 40 GB memory. Our model development was performed on a Linux Ubuntu v20.04.6 LTS environment, with Python v3.8.10, Anaconda v4.9.2, CUDA v11.8.0, CUDNN v8.8.0.121-11.8, PyTorch v1.13.1, PyTorch Lightning v1.1.0, and Sigpy v0.1.25.

## Results

### Retrospective study

Figure 2 depicts reconstructions for retrospective undersampling with R=6 at 3T and 0.55T with PSNR and SSIM metrics related to GRAPPA reconstruction at R=2. The top row of each subfigure presents MIP

views. The red boxes on the MIP images determine the view of the cropped MIP images in the second row. The last row shows representative slices showing differences in interesting anatomical details. Note that the metrics are calculated on 3-D volumes, not on MIP images. In Figure 2(a), which includes results from the 3T system, VN achieves PSNR [dB]/SSIM [%] of 39.74/92.15, while CG-SENSE, CS, and SSDU show values of 28.82/47.92, 34.99/80.97, and 36.14/83.71, respectively. In addition, looking at the green circles of Figure 2(a), VN removes aliasing artifacts while the other reconstructions suffer from them. Furthermore, the orange circles of Figure 2(a) indicates that VN displays the sharper gallbladder and common bile duct. In Figure 2(b) showing 0.55T results, VN achieves PSNR [dB]/SSIM [%] of 34.20/80.66, CS-SENSE 24.44/31.93, CS 30.76/64.68, and SSDU 31.40/67.32. The blue circles of Figure 2(b) demonstrate that VN efficiently suppresses the background noise while presenting hepatobiliary ducts.

Figure 3 contains violin plots of metric scores, such as PSNR in dB and SSIM in %, across two MRI scanner systems. These metric scores are computed from eight volunteers at 3T and four volunteers at 0.55T in the test dataset. VN shows the highest median values and the narrowest interquartile ranges for both PSNR and SSIM metrics, indicating superior performance and consistency across measurements when compared with CG-SENSE, CS, and SSDU. SSDU performs slightly better than CS for both field strengths. However, SSDU shows large variability, especially for the data from 3T. CG-SENSE performs worst in all experiments. Table 2 summarizes the average PSNR and SSIM of the test dataset with the corresponding  $p$ -values at 3T and 0.55T. VN consistently exhibits the highest metrics for both field strengths. On the 3T system, the t-Test results between VN and the other reconstructions indicate statistical significance, as all  $p$ -values are below 0.05.

Figure 4 shows the line profiles at the end of the common bile duct. The representative position of the line profile is shown as the red arrow in Figure 2(a), and the same position applies to respective reconstructions. The line profile of VN is very close to the ground truth (GRAPPA) and shows the highest PPCMM of 0.96. Notably, the green arrow in Figure 4 demonstrates that both GRAPPA and VN accurately reconstruct a small duct, while the other reconstructions fail to do so. In addition, CG-SENSE and CS produce unexpected peaks that are not present in the ground truth as pointed by the blue arrow in Figure 4. SSDU, on the other hand, merges two peaks (see two pink circles in Figure 4) into one indicated by the pink arrow in Figure 4.

### Prospective study

Table 1 includes required breathing cycles and actual acquisition time (TA). MRCP acquisitions at R=2 for 3T and 0.55T require 97 and 82 breathing cycles, respectively. The number of these cycles corresponds to an estimated time of 303 and 249 seconds, respectively. In contrast, MRCP acquisitions at R=6 for both field strengths require only 39 and 38 cycles, corresponding to 138 and 139 seconds, respectively. The same tendency is observed for TA, showing that the average TAs of 3T and 0.55T at R=2 are 599 and 542 seconds, respectively, while those at R=6 are 255 and 180 seconds.

Figure 5 depicts the results of reconstructions for prospective undersampling with R=6 for 3T and 0.55T. All reconstructions with the exception of the VN show aliasing artifacts in the green circles of Figure 5(a). In the blue circles of Figure 5(b), fine hepatobiliary ducts, which are removed in SSDU and buried under the noise level in CG-SENSE are visible in the VN reconstruction.

Figure 6 shows the line profiles of reconstructions for prospective undersampling at R=6. The blue arrow in Figure 6 indicates that the line profile of VN clearly removes aliasing artifacts, while significant deviations are observed with other methods.

## Discussion

The goal of our study was the reduction of scan time for PACE-MRCP acquisitions with the use of DL reconstruction. We achieved the high-speed PACE-MRCP acquisitions by undersampling three times more than in the clinical applications, i.e., increasing the acceleration factor from R=2 to R=6. More specifically, the TAs at R=6 are 2.4 and 3.0 times faster than those at R=2 for 3T and 0.55T, respectively. It means that our method boosts MRCP acquisition at least more than twice in time. At the same time, we alleviated the side effects such as aliasing artifacts and noise amplification, caused by undersampling with the high acceleration factor using DL reconstruction. Our prospective experiments demonstrate that our DL reconstructions can be applied in real-world applications beyond retrospective simulations.

One interesting finding of our experiments was that in contrast to recent results from the literature [15], supervised VN trainings using GRAPPA reconstructions of R=2 undersampled acquisitions consistently outperformed self-supervised trainings directly on the undersampled data (SSDU). One possible explanation is that in our experimental design, the acceleration factor for our parallel imaging ground truth reconstructions followed the standard clinical MRCP protocol and therefore was relatively low (R=2). As a consequence, our GRAPPA reconstructions yielded clinically acceptable image quality without significant artifacts or noise amplification.

One open question in the field of deep learning MR image reconstruction is the generalization of a single model with respect to changes in the image acquisition setup. In our experimental design, we tested this by training our deep learning model on 3T and then applying it to data acquired at 0.55T experiment. Our results show that even with this domain shift between training and testing, the data-driven deep learning models consistently outperform compressed sensing and parallel imaging.

## Conclusion

We have achieved a significant reduction in acquisition time for PACE-MRCP with DL reconstruction. Our results demonstrate superior performance in comparison to other reconstructions, such as parallel imaging, compressed sensing, and self-supervised DL reconstruction, for both retrospectively and prospectively accelerated acquisitions, as well as generalizability across field strengths from 3T to 0.55T.

## Acknowledgements

This work is supported by the Erlangen National High Performance Computing Center (NHR@FAU) of Friedrich-Alexander-Universität Erlangen-Nürnberg (FAU) under the NHR project b143dc. NHR funding is provided by federal and Bavarian state authorities. NHR@FAU hardware is partially funded by the German Research Foundation (DFG) – 440719683. The authors thank Thomas Benkert, Bruno Riemenschneider, Zhengguo Tan, and Marc Vornehm for the beneficial discussion and technical supports.

## Conflict of Interest Statement

J.K. receives a PhD stipend from Siemens Healthineers AG. M.D.N. is employed by Siemens Healthineers AG. F.K. receives research support from Siemens Healthineers AG and has stock options from Subtle Medical.

## Data Availability Statement

The Python implementations of the reconstruction framework with sample dataset are available to any interested researchers ([https://github.com/JinhoKim46/MRCP\\_DLRecon](https://github.com/JinhoKim46/MRCP_DLRecon)).

## Funding Information

DFG, Grant/Award Number: 513220538; NIH, Grant/Award Number: R01EB024532, P41EB017183

## Figures

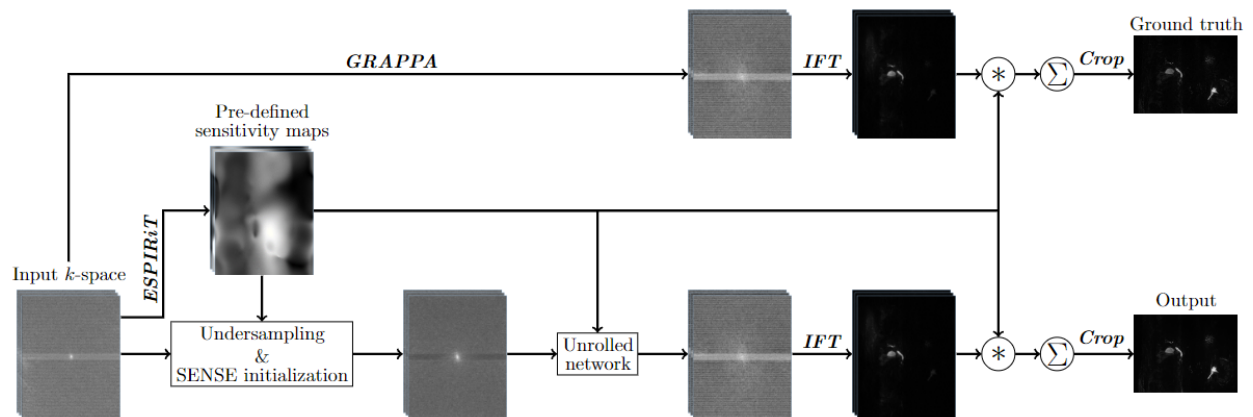


Figure 1: Training pipeline: GRAPPA reconstructions from two-fold accelerated data are used as the ground truth for supervised training. A SENSE reconstruction is applied to the retrospectively six-fold accelerated data to generate the input to the unrolled network. The architecture of the unrolled network is based on the VN. The same pre-defined ESPIRiT-based sensitivity maps are used for GRAPPA reconstructions and output of the network.

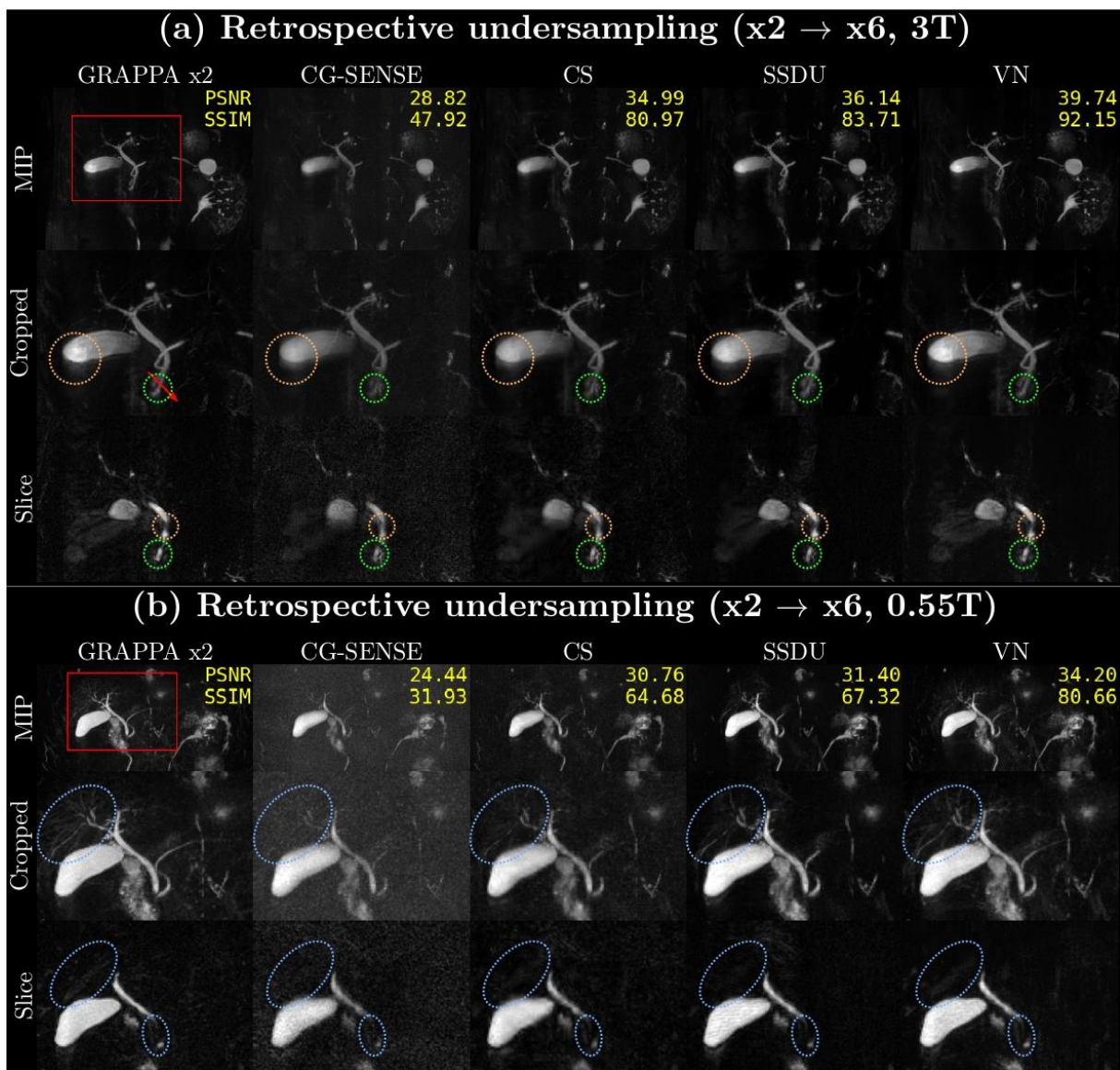
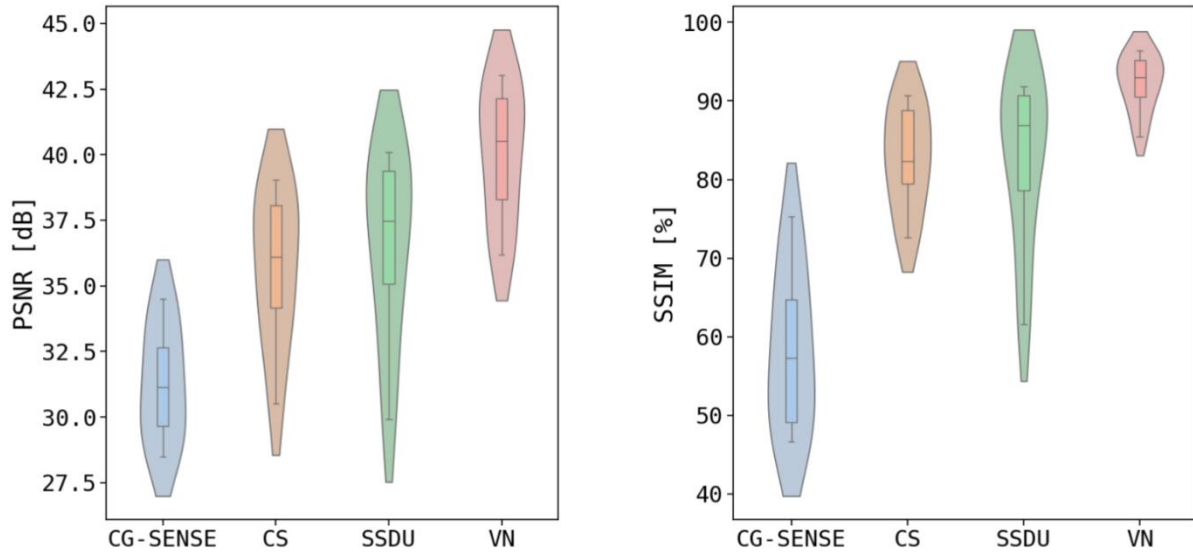
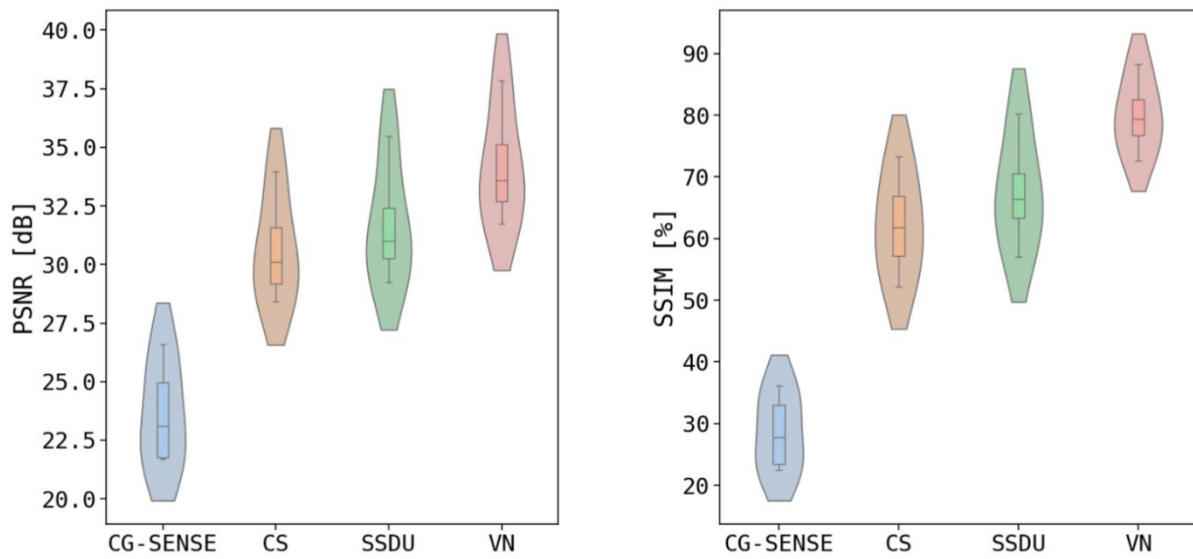


Figure 2: Results of retrospective undersampling at (a) 3T and (b) 0.55T: We use GRAPPA with a two-fold acceleration as the ground truth for comparison with CG-SENSE, CS, SSDU, and VN reconstructions with a six-fold acceleration. Each column corresponds to a reconstruction method and shows three different presentation forms: Maximum Intensity Projection (MIP) (top), a cropped view of the hepatobiliary duct of the MIP (middle), and a representative single slice (bottom). In (a), the green circles indicate aliasing artifacts, and the orange circles display the representative sharpness of the gallbladder and the common bile duct. In (b), the blue circles show fine details of the hepatobiliary ducts. The MIP images of the six-fold reconstructions are quantitatively assessed with PSNR in dB and SSIM in % with respect to GRAPPA  $x2$ . The red arrow in (a) indicates the signal intensity source for the line profile representation for Figure 4.



(a) 3T scanner system



(b) 0.55T scanner system

Figure 3: Violin plots of PSNR in dB and SSIM in % of the different reconstruction methods against the R=2 GRAPPA reconstructions for (a) 3T (eight test set subjects) and (b) 0.55T (four test set subjects). Within each graph, box plots are included to provide a visual representation of the data distribution range.

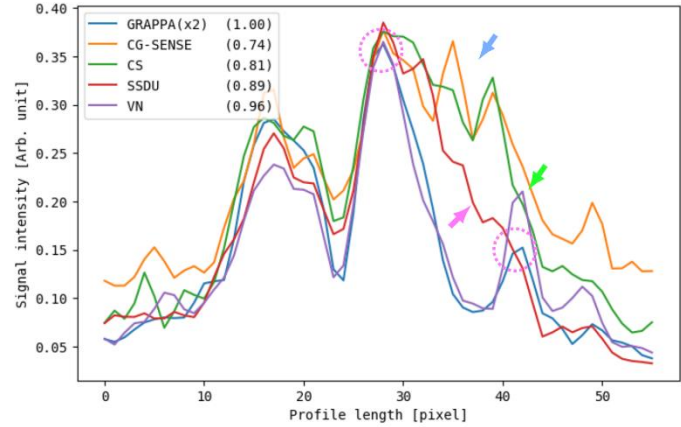


Figure 4: Line profiles from the retrospective study. The line profiles are taken from the same position of the corresponding reconstructions, respectively, and one representative position is presented as the red arrow in Figure 2(a). Pearson product-moment correlation coefficients (PPMCC) against GRAPPA(x2) are shown in the legend for the corresponding reconstructions to quantify the similarity to the reference profile. VN presents the highest PPMCC among others, meaning that the line profile of VN is the most similar to GRAPPA(x2). The green arrow indicates that only VN can reconstruct the small duct precisely. The blue arrow points to where CG-SENSE and CG fail to reconstruct the image correctly. In addition, the pink arrow demonstrates that SSDU merges two peaks (pink circles) into one.

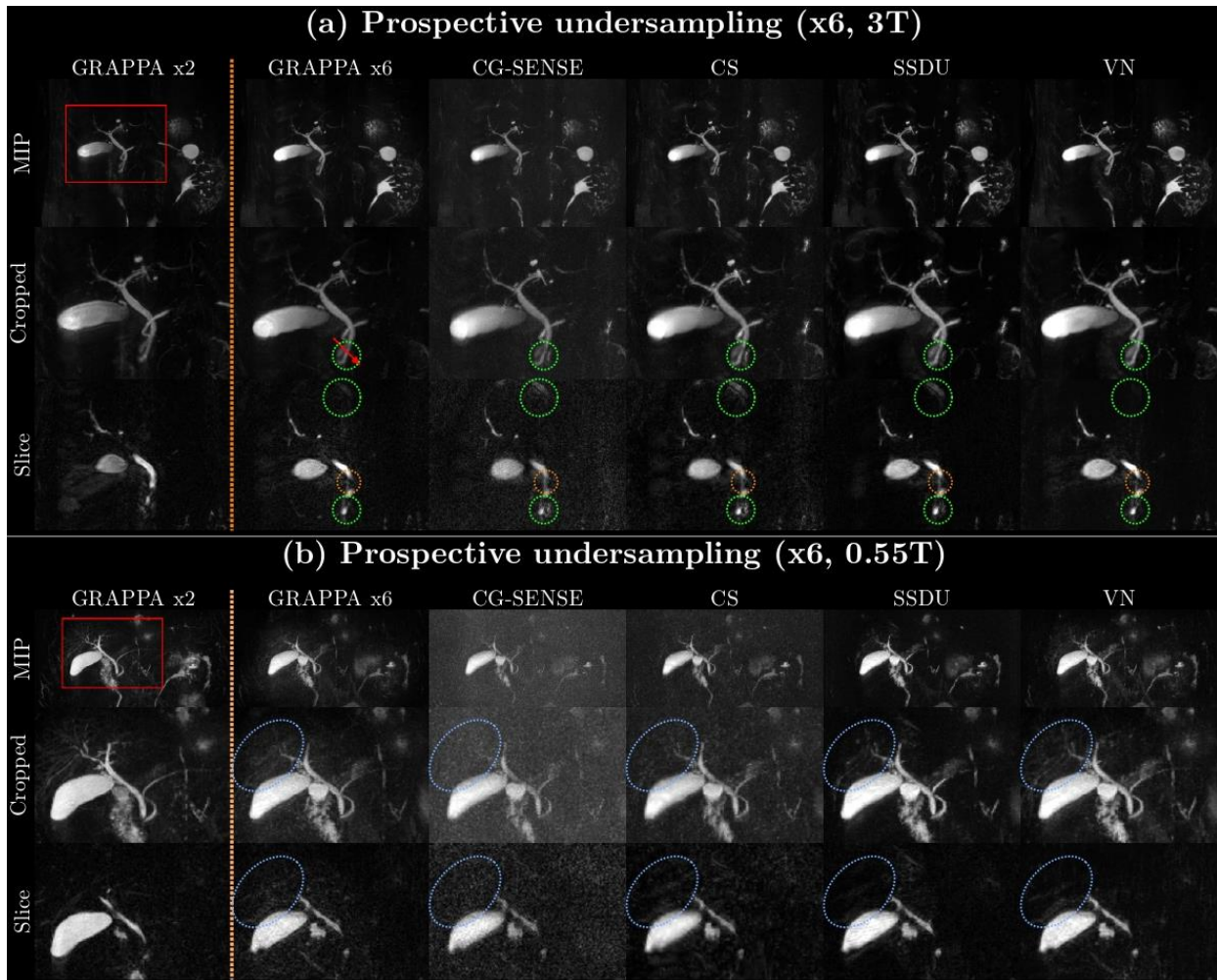


Figure 5: Results of prospective undersampling at (a) 3T and (b) 0.55T: We use GRAPPA with a two-fold acceleration to serve as a reference. Then we reconstruct six-fold prospective undersampling using GRAPPA, CG-SENSE, CS, SSDU, and VN approaches. Each column corresponds to one reconstruction method and shows three different presentation forms: Maximum Intensity Projection (MIP) (top), a cropped view of the hepatobiliary duct of the MIP (middle), and a representative single slice (bottom). In (a), the green circles indicate aliasing artifacts, and the orange circles represent the sharpness of the anatomical regions. In (b), the blue circles show fine details of the hepatobiliary ducts. The red arrow in (a) indicates the signal intensity source for the line profile representation for Figure 6.

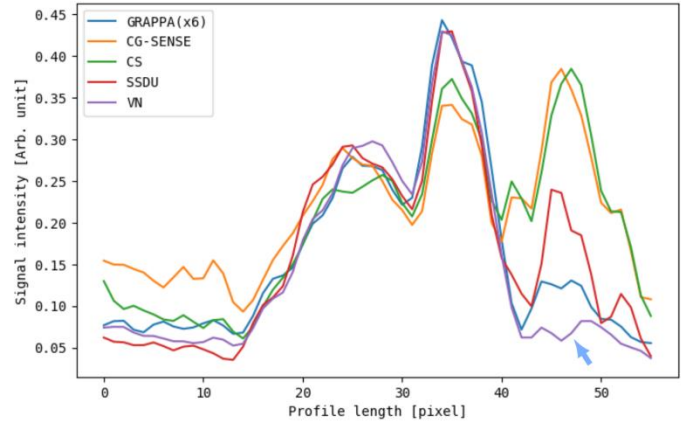


Figure 6: Line profiles from the prospective study. The line profiles are taken from the same position of the corresponding reconstructions, respectively, and one representative position is presented as the red arrow in Figure 5(a). The blue arrow points to where VN removes aliasing artifacts successfully.

## Tables

Table 1: Parameters for MRI protocols

Parameters	3T		0.55T	
Scanner	MAGNETOM Vida & Lumina		MAGNETOM Free.Max	
Sequence	3-D T2-weighted TSE (SPACE) [20]			
Acquisition plane	Coronal			
Turbo factor	180			
TR [ms]*	5985 ± 2103 (2700–12829)		5298 ± 1462 (4251–8878)	
TE [ms]*	703 ± 2 (701–709)		703	
Acquired voxel size [mm <sup>3</sup> ]	0.5 × 0.5 × 1.2		0.7 × 0.7 × 1.0	
Matrix	384 × 480		256 × 194	
Number of slices	64			
Flip angles*	115, 120		145	
Echo train spacing [ms]	5.26		5.58	
Echo train duration [ms]	957		1016	
Number of signal averages	1.4		2	
Bandwidth [Hz/pixel]	352		391	
Triggering	PACE signal			
Number of ACS	24			
Undersampling pattern	Cartesian			
Acceleration - slice	x1			
Acceleration - PE	x2	x6	x2	x6
Breathing cycles (estim. time [s])	97 (303)	39 (138)	82 (249)	38 (139)
TA [s]*	599 ± 283 (229–1386)	255 ± 81 (161–426)	542 ± 172 (370–720)	180 ± 28 (158–226)

TSE, turbo spin-echo; TR, repetition time; TE, echo time; ACS, autocalibration signal; PE, phase encoding; TA, acquisition time.

The notation format for TR, TE, and TA is Mean ± Standard deviation (Minimum – Maximum).

\* Variable depending on the volunteer.

Table 2: Quantitative analysis of the retrospective study at R=6

		CG-SENSE	CS	SSDU	VN	p-value		
						CG-SENSE vs. VN	CS vs. VN	SSDU vs. VN
3T	PSNR	31.27 ± 2.11	35.74 ± 2.77	36.58 ± 3.39	<b>40.07 ± 2.46</b>	< 0.001*	0.008*	0.045*
	SSIM	58.27 ± 9.74	82.76 ± 6.21	82.70 ± 10.23	<b>92.26 ± 3.47</b>	< 0.001*	0.003*	0.034*
0.55T	PSNR	23.62 ± 2.03	30.65 ± 2.10	31.67 ± 2.32	<b>34.20 ± 2.28</b>	0.001*	0.094	0.227
	SSIM	28.55 ± 5.70	62.23 ± 7.77	67.52 ± 8.33	<b>79.90 ± 5.64</b>	< 0.001*	0.019*	0.077

CG-SENSE, conjugate gradient SENSE; CS, compressed sensing; SSDU, self-supervised learning via data undersampling; VN, variational network; PSNR, peak signal-to-noise ratio; SSIM, structural similarity.

The notation format for PSNR and SSIM is Mean ± Standard deviation.

PSNR and SSIM are averaged over eight test data for 3T and four for 0.55T.

\* p-value < 0.05 is considered statistically significant.

## References

- [1] M. A. Barish, E. K. Yucel and J. T. Ferrucci, "Magnetic resonance cholangiopancreatography," *New England Journal of Medicine*, vol. 341, no. 4, pp. 258-264, 1999.
- [2] H. Irie, H. Honda, T. Tajima, T. Kuroiwa, K. Yoshimitsu, K. Makisumi and K. Masuda, "Optimal MR cholangiopancreatographic sequence and its clinical application," *Radiology*, vol. 206, no. 2, pp. 379-387, 1998.
- [3] A. S. Fulcher, M. A. Turner and G. W. Capps, "MR Cholangiography: Technical Advances and Clinical Applications," *Radiographics*, vol. 19, no. 1, pp. 25-44, 1999.
- [4] S. Nagata, S. Goshima, Y. Noda, N. Kawai, K. Kajita, H. Kawada, Y. Tanahashi and M. Matsuo, "Possible biliary disease: Diagnostic performance of high-spatial-resolution isotropic 3D T2-weighted MRCP," *Radiology*, vol. 249, no. 3, pp. 883-890, 2008.
- [5] L. S. Yoon, O. A. Catalano, S. Fritz, C. R. Ferrone, P. F. Hahn and D. V. Sahani, "Another Dimension in Magnetic Resonance Cholangiopancreatography: Comparison of 2-and 3-Dimensional Magnetic Resonance Cholangiopancreatography for the Evaluation of Intraductal Papillary Mucinous Neoplasm of the Pancreas," *Journal of computer assisted tomography*, vol. 33, no. 3, pp. 363-368, 2009.
- [6] S. Morita, E. Ueno, K. Suzuki, H. Machida, M. Fujimura, S. Kojima, M. Hirata, T. Ohnishi and C. Imura, "Navigator-triggered prospective acquisition correction (PACE) technique vs. conventional respiratory-triggered technique for free-breathing 3D MRCP: An initial prospective comparative study using healthy volunteers," *Journal of Magnetic Resonance Imaging: An Official Journal of the International Society for Magnetic Resonance in Medicine*, vol. 28, no. 3, pp. 679-677, 2008.
- [7] P. Asbach, C. Klessen, T. J. Kroencke, C. Kluner, A. Stemmer, B. Hamm and M. Taupitz, "Magnetic resonance cholangiopancreatography using a free-breathing T2-weighted turbo spin-echo sequence with navigator-triggered prospective acquisition correction," *Magnetic resonance imaging*, vol. 23, no. 9, pp. 939-945, 2005.
- [8] B. Sun, Z. Chen, Q. Duan, Y. Xue, E. Zheng, Y. He, L. Lin, G. Li and Z. Zhang, "Rapid 3D navigator-triggered MR cholangiopancreatography with SPACE sequence at 3T: only one-third acquisition time of conventional 3D SPACE navigator-triggered MRCP," *Abdominal Radiology*, vol. 45, no. 1, pp. 134-140, 2020.
- [9] S. Nagata, S. Goshima, Y. Noda, N. Kawai, K. Kajita, H. Kawada, Y. Tanahashi and M. Matsuo, "Magnetic resonance cholangiopancreatography using optimized integrated combination with parallel imaging and compressed sensing technique," *Abdominal Radiology*, vol. 44, pp. 1766-1772, 2019.
- [10] J. H. Yoon, S. M. Lee, H. J. Kang, E. Weiland, E. Raithel, Y. Son, B. Kiefer and J. M. Lee, "Clinical Feasibility of 3-Dimensional Magnetic Resonance Cholangiopancreatography Using Compressed

- Sensing: Comparison of Image Quality and Diagnostic Performance," *Investigative radiology*, vol. 52, no. 10, pp. 612-619, 2017.
- [11] K. P. Pruessmann, M. Weiger, M. B. Scheidegger and P. Boesiger, "SENSE: Sensitivity encoding for fast MRI," *Magnetic Resonance in Medicine: An Official Journal of the International Society for Magnetic Resonance in Medicine*, vol. 42, no. 5, pp. 952-962, 1999.
- [12] M. Lustig, D. Donoho and J. M. Pauly, "Sparse MRI: The application of compressed sensing for rapid MR imaging," *Magnetic Resonance in Medicine: An Official Journal of the International Society for Magnetic Resonance in Medicine*, vol. 58, no. 6, pp. 1182-1195, 2007.
- [13] C. M. Hyun, H. P. Kim, S. M. Lee, S. Lee and J. K. Seo, "Deep learning for undersampled MRI reconstruction," *Physics in Medicine & Biology*, vol. 63, no. 13, p. 135007, 2018.
- [14] K. Hammernik, T. Klatzer, E. Kobler, M. P. Recht, D. K. Sodickson, T. Pock and F. Knoll, "Learning a variational network for reconstruction of accelerated MRI data," *Magnetic resonance in medicine*, vol. 79, no. 6, pp. 3055-3071, 2018.
- [15] B. Yaman, S. A. H. Hosseini, S. Moeller, J. Ellermann, K. Uğurbil and M. Akçakaya, "Self-supervised learning of physics-guided reconstruction neural networks without fully sampled reference data," *Magnetic resonance in medicine*, vol. 84, no. 6, pp. 3172-3191, 2020.
- [16] F. Knoll, K. Hammernik, E. Kobler and D. K. Sodickson, "Assessment of the generalization of learned image reconstruction and the potential for transfer learning," *Magnetic resonance in medicine*, vol. 81, no. 1, pp. 116-128, 2019.
- [17] J. P. Marques, F. F. Simonis and A. G. Webb, "Low-field MRI: An MR physics perspective," *Journal of magnetic resonance imaging*, vol. 49, no. 6, pp. 1528-1542, 2019.
- [18] M. Akçakaya, S. Nam, P. Hu, M. H. Moghari, L. H. Ngo, V. Tarokh, W. J. Manning and R. Nezafat, "Compressed sensing with wavelet domain dependencies for coronary MRI: A retrospective study," *IEEE Transactions on Medical Imaging*, vol. 30, no. 5, pp. 1090-1099, 2011.
- [19] K. P. Pruessmann, M. Weiger, P. Börnert and P. Boesiger, "Advances in sensitivity encoding with arbitrary k-space trajectories," *Magnetic Resonance in Medicine: An Official Journal of the International Society for Magnetic Resonance in Medicine*, vol. 46, no. 4, pp. 638-651, 2001.
- [20] S. Diamond, V. Sitzmann, F. Heide and G. Wetzstein, "Unrolled optimization with deep priors," *arXiv preprint arXiv:1705.08041*, 2017.
- [21] M. P. Lichy, B. M. Wietek, J. P. Mugler, W. Horger, Marion, I. Menzel, A. Anastasiadis, K. Siegmann, T. Niemeyer, A. Königsrainer, B. Kiefer, F. Schick, C. D. Claussen and H.-P. Schlemmer, "Magnetic Resonance Imaging of the Body Trunk Using a Single-Slab, 3-Dimensional, T2-weighted Turbo-Spin-Echo Sequence With High Sampling Efficiency (SPACE) for High Spatial Resolution Imaging Initial Clinical Experiences," *Investigative Radiology*, vol. 40, pp. 756-760, 2005.

- [22] J. P. Mugler, "Optimized three-dimensional fast-spin-echo MRI," *Journal of Magnetic Resonance Imaging*, vol. 39, no. 4, pp. 745-767, 2014.
- [23] S. J. Inati, J. D. Naegele, N. R. Zwart, V. Roopchansingh, M. J. Lizak, D. C. Hansen, C.-Y. Liu, D. Atkinson, P. Kellman, S. Kozerke and others, "ISMRM Raw data format: A proposed standard for MRI raw datasets," *Magnetic resonance in medicine*, vol. 77, no. 1, pp. 411-421, 2017.
- [24] M. Uecker, P. Lai, M. J. Murphy, P. Virtue, M. Elad, J. M. Pauly, S. S. Vasanawala and M. Lustig, "ESPIRiT - An eigenvalue approach to autocalibrating parallel MRI: Where SENSE meets GRAPPA," *Magnetic resonance in medicine*, vol. 71, no. 3, pp. 990-1001, 2014.
- [25] F. Ong and M. Lustig, "SigPy: a python package for high performance iterative reconstruction," in *Proceedings of the ISMRM 27th Annual Meeting*, 2019.
- [26] M. A. Griswold, P. M. Jakob, R. M. Heidemann, M. Nittka, V. Jellus, J. Wang, B. Kiefer and A. Haase, "Generalized Autocalibrating Partially Parallel Acquisitions (GRAPPA)," *Magnetic Resonance in Medicine: An Official Journal of the International Society for Magnetic Resonance in Medicine*, vol. 47, no. 6, pp. 1202-1210, 2002.
- [27] O. Ronneberger, P. Fischer and T. Brox, "U-net: Convolutional networks for biomedical image segmentation," in *Medical Image Computing and Computer-Assisted Intervention–MICCAI 2015: 18th International Conference*, 2015.
- [28] K. He, X. Zhang, S. Ren and J. Sun, "Deep Residual Learning for Image Recognition," *Proceedings of the IEEE conference on computer vision and pattern recognition*, pp. 770-778, 2016.
- [29] K. Pearson, "Notes on the history of correlation," *Biometrika*, vol. 13, no. 1, pp. 25-45, 1920.
- [30] Z. Kotevski and P. Mitrevski, "Experimental Comparison of PSNR and SSIM Metrics," in *International Conference on ICT Innovations*, 2009.
- [31] T. Akiba, S. Sano, T. Yanase, T. Ohta and M. Koyama, "Optuna: A Next-generation Hyperparameter Optimization Framework," in *Proceedings of the 25th ACM SIGKDD international conference on knowledge discovery & data mining*, 2019.
- [32] T. Matsuyama, Y. Ohno, K. Yamamoto, M. Ikedo, M. Yui, M. Furuta, R. Fujisawa, S. Hanamatsu, H. Nagata, T. Ueda and others, "Comparison of utility of deep learning reconstruction on 3D MRCPs obtained with three different k-space data acquisitions in patients with IPMN," *European Radiology*, vol. 32, no. 10, pp. 6658-6667, 2022.
- [33] K. Shiraishi, T. Nakaura, H. Uetani, Y. Nagayama, M. Kidoh, N. Kobayashi, K. Morita, Y. Yamahita, Y. Tanaka, H. Baba and others, "Deep learning-based reconstruction and 3D hybrid profile order technique for MRCP a 3T: evaluation of image quality and acquisition time," *European Radiology*, pp. 1-10, 2023.
- [34] B. Tins, V. Cassar-Pullicino, M. Haddaway and U. Nachtrab, "Three-dimensional sampling perfection with application-optimised contrasts using a different flip angle evolutions sequence for

routine imaging of the spine: Preliminary experience," *The British Journal of Radiology*, vol. 85, no. 1016, pp. e480-e489, 2012.

- [35] Y. Zhang, W. Peng, Y. Xiao, Y. Ming, K. Ma, S. Hu, W. Zeng, L. Zeng, Z. Liang, X. Zhang and others, "Rapid 3D breath-hold MR cholangiopancreatography using deep learning-constrained compressed sensing reconstruction," *European Radiology*, vol. 33, no. 4, pp. 2500-2509, 2023.